Phase-separation-induced changes in the magnetic and transport properties of the quaternary Heusler alloy $Co_2Mn_{1-x}Ti_xSn$

Tanja Graf, Joachim Barth, Christian G. F. Blum, Benjamin Balke, and Claudia Felser*
Institut für Anorganische und Analytische Chemie, Johannes Gutenberg-Universtität, 55099 Mainz, Germany

Peter Klaer and Hans-Joachim Elmers
Institut für Physik, Johannes Gutenberg-Universtität, 55099 Mainz, Germany
(Received 15 June 2010; published 17 September 2010)

The quaternary Heusler compound $Co_2Mn_{1-x}Ti_xSn$ with $x=0$, 0.2, 0.4, 0.5, 0.6, 0.8, and 1 shows a phase separation into the two Heusler compounds, Co_2MnSn and Co_2TiSn. Only at the edges of the composition range a slight admixture of Mn and Ti to the respective other phase is observed. This phase separation leads to a distinct microstructure which can be altered by the composition of the material. Pronounced changes in the magnetic and electronic properties take place with varying composition. Two magnetic transitions occur which indicate different Curie temperatures for both phases. The reduction in the thermal lattice conductivity is of particular interest for an optimization of Heusler compounds for thermoelectric applications. In the field of spintronics the use of superlattices composed of Co_2MnSn and Co_2TiSn without any interlayer diffusion is suggested.

DOI: 10.1103/PhysRevB.82.104420 PACS number(s): 61.66.Dk, 64.75.Nx, 72.15.Eb, 75.50.Cc

I. INTRODUCTION

Half-metallic ferromagnets have been proposed to be ideal candidates for spin injection devices because they exhibit 100% spin polarization at the Fermi energy ϵ_F.[1,2] In the recent past Heusler compounds have attracted great interest in this context.[3,4] For Co_2-based Heusler compounds half metallicity was predicted by Kübler *et al.* already in 1983.[5] A great advantage of those compounds is the possibility to specifically tune the position of the Fermi level and thus their electronic and magnetic properties by partial substitution of elements in the parent phase.[6–9] The preservation of half metallicity was confirmed by density-functional theory calculations for quaternary alloys of the types $(XX')_2YZ$, $X_2YY'Z$, and X_2YZZ'.[10] Furthermore, many Heusler compounds exhibit high Curie temperatures which is an important requirement for the application of the material in electromagnetic devices.[11–14] The half metallicity was experimentally demonstrated for the compound $Co_2FeAl_{0.5}Si_{0.5}$, even at room temperature.[15] For this material high tunnel magnetoresistance (TMR) ratios of 386% at room temperature were reached recently.[16]

Despite these promising results one has to be aware of a possible solubility gap and phase-separation phenomena in thermal equilibrium which may occur due to the substitution of elements. Experimental evidence for an enhancement of the spin-polarization despite of phase-separation phenomena was reported for the system $Co_2MnAl_{(1-x)}Sn_x$.[17] Theoretical studies predict the spinodal decomposition of the Half-Heusler alloy $CoTi_{(1-x)}Fe_xSb$.[18] Phase-separation and interdiffusion effects play a major role for the performance of TMR devices, e.g., Mn diffusion from the IrMn pinning layer into the ferromagnetic electrodes reduces the TMR ratio significantly above a critical annealing temperature.[19] Additionally, phase separations have a major impact in the field of thermoelectrics. Microstructuring of thermoelectric materials leads to a reduction in the thermal conductivity, and thus, is one method to optimize the thermoelectric figure of merit *ZT*.

In this study, the phase separation appearing in the quaternary Heusler series $Co_2Mn_{1-x}Ti_xSn$ is reported. The quaternary compounds have a dendritic microstructure which was formed during the solidification process as a result of a phase separation into a Co_2MnSn-enriched and a Co_2TiSn-enriched Heusler phases (below shortened as Mn and Ti enriched). The impact of this phase separation on the magnetic and transport properties was studied in detail.

II. EXPERIMENTAL DETAILS

Polycrystalline ingots of the compounds were prepared by arc melting of stoichiometric amounts of high-purity elements in an argon atmosphere to avoid oxygen contamination at a pressure of 10^{-4} mbar. Additionally, a Ti sponge was used to bind remaining oxygen. The samples were melted three times. They were turned over after each melting process to yield a homogeneous sample. The weight loss after the whole melting procedure was less than 1%. The polycrystalline ingots were annealed in an evacuated quartz tube at 1073 K for 2 weeks.

The crystallographic structure was investigated by x-ray powder diffraction using Mo $K\alpha$ radiation ($\lambda = 0.7093165$ nm; Bruker, AXS D8) in reflection geometry. The experimental diffraction patterns were refined using the FULLPROF program.[20] Complementary, x-ray diffraction (XRD) experiments were performed at the XRD beamline at the bending magnet D10 of the Brazilian Synchrotron Light Laboratory (LNLS; used wavelength $\lambda = 1.75872$ Å). For details about the characteristics of the beamline see Ref. 21.

A scanning electron microscope (SEM, Jeol JSM-6400) equipped with an energy-dispersive x-ray spectroscopy (EDX) detection system (EUMEX EDX) was used to check the homogeneity and stoichiometry of the samples. The measurements were carried out at a pressure of 3×10^{-6} mbar.

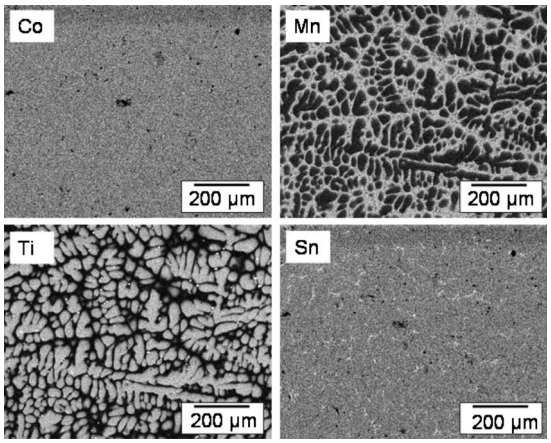

FIG. 1. Element-sensitive EDX scans of the compound $Co_2Mn_{0.5}Ti_{0.5}Sn$.

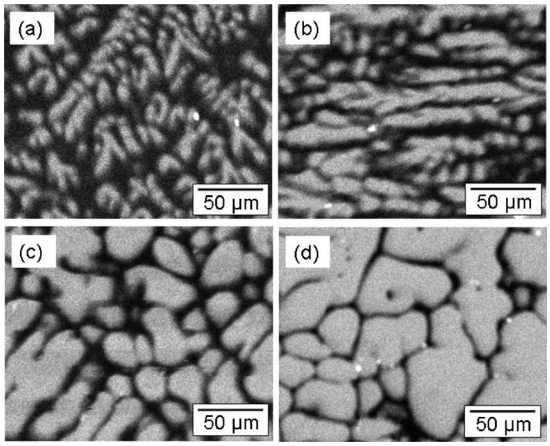

FIG. 2. Element distribution of (a) $Co_2Mn_{0.8}Ti_{0.2}Sn$, (b) $Co_2Mn_{0.6}Ti_{0.4}Sn$, (c) $Co_2Mn_{0.4}Ti_{0.6}Sn$, and (d) $Co_2Mn_{0.2}Ti_{0.8}Sn$. Light areas are Ti-enriched, dark areas are Mn enriched.

An acceleration voltage of 20 kV was applied and an inspection angle of 35° was setup. For the correction of the quantitative data the *ZAF* method was applied which relies on atomic number (*Z*), absorption (*A*), and fluorescence (*F*) effects. The images were acquired via the digital image processing system and the quantitative chemical analysis was performed with the program WINEDS 4.0.

The magnetic properties were investigated by a superconducting quantum interference device (SQUID) (Quantum Design, Magnetic Property Measurement System XL-5) using nearly spherical pieces of approximately 5–10 mg of the samples. Measurements of the Seebeck coefficient, the resistivity and the thermal conductivity were performed with a physical property measurement system (Model 6000, Quantum System, with the options P400, P600, and P640) from 2 to 400 K. The samples were cut into bars with the approximate dimensions $2\times2\times10$ mm^3. The samples were polished before contacting in order to remove oxide layers that may have formed during synthesis and the measurement. The bars have been contacted with four copper stripes that were wrapped around the bars to homogenize the current passing through. The sample chamber was flooded with helium and evacuated afterwards. The measurements were carried out at a pressure of 1.2×10^{-4} mbar by a standard four-point ac method. An additional correction term for the heat loss at the heating shoes was introduced and applied to the thermal conductivity data as suggested by Müller *et al.*[22] and Quantum Design.[23]

III. RESULTS

A. Phase separation

The distribution of the different elements and the homogeneity of the samples was investigated by EDX. Figure 1 shows element-resolved pictures of $Co_2Mn_{0.5}Ti_{0.5}Sn$. Cobalt and tin are homogeneously distributed over the investigated area. Manganese and titanium, however, are distributed inhomogeneously into Mn-enriched areas which contain hardly any titanium and Ti-enriched areas with only small amounts of manganese. Figure 2 shows only the Ti-sensitive pictures of $x=0.2$, 0.4, 0.6, and 0.8, the remaining pictures were omitted for reasons of clarity. It can be seen that the size and the shape of the microstructure change with the composition of the sample. On the Mn-rich side of the composition series the microstructure is diffuse [Figs. 2(a) and 2(b)] and the boundaries are weakly pronounced. Very sharp boundaries are obtained for the Ti-rich part as displayed in Figs. 2(c) and 2(d). From the morphology of the phase-separated areas one may conclude that the bulky Ti-rich areas nucleate first out of the liquid phase during cooling. Only after nearly all Ti is solidified in the Ti-rich phase the remaining Mn forms a solidified Co_2MnSn matrix. The observed morphology may thus be taken as a hint to phase separation by nucleation and growth in contrast to a spinodal decomposition. This consideration is in good agreement with the higher melting temperature of Co_2TiSn ($\approx$1460 K) in contrast to Co_2MnSn ($\approx$1250 K). Scans along arbitrarily chosen lines were performed. As an example, the element distribution of $Co_2Mn_{0.4}Ti_{0.6}Sn$ is shown in Fig. 3. This investigation shows that the Mn and Ti concentration complement one another. The composition of each phase was determined by EDX and is given in Table I. A graphic representation of the composition of the Mn-rich phase (squares) and the Ti-rich phase (circles) for the whole alloyed system from Co_2MnSn to Co_2TiSn is displayed in Fig. 4. Full and open symbols denote the Mn and Ti concentration in each phase, respectively. The Mn-rich phase mainly consists of Co_2MnSn for $x\leq0.6$, only for $x=0.8$ it contains $\sim$60% Ti. The Ti-rich phase is comprised of $Co_2Mn_xTi_ySn$, whereby the amount of Mn in this phase increases with rising Mn content in the sample. Only on the very Ti-rich side of the composition range, a pure Co_2TiSn phase is obtained.

X-ray diffraction with Mo $K\alpha$ radiation yields diffraction patterns which indicate $L2_1$-ordered compounds, no secondary phases were observed. The data were refined using the Rietveld method and are displayed in Fig. 5(a). The lattice parameters vary from 6.01 to 6.06 Å with increasing amount of Ti as expected from the larger atomic radius of Ti [compare Fig. 5(b)]. The deviations from the linear behavior may be explained by the fact that the phases do not consist purely

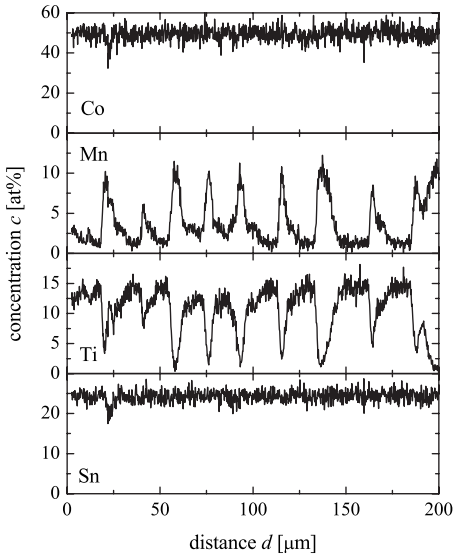

FIG. 3. Concentration of indicated elements along a line on the surface of $Co_2Mn_{0.4}Ti_{0.6}Sn$ determined by EDX.

of the ternary compounds. Especially the Ti-rich phase contains a considerable amount of Mn which might lead to these nonlinear deviations. The expected splitting of the reflections due to the different lattice parameters of the two phases could not be resolved by the laboratory method because of the present $K\alpha 1/K\alpha 2$ splitting. Therefore, further XRD measurements were carried out at the synchrotron. To obtain a high resolution an additional Ge (111)-analyzer crystal leads to a sharp instrumental angular resolution, $\Gamma(2\theta) \approx 0.015°$ at the measured angle of around $2\theta = 50°$, and efficiently removes unwanted fluorescence and air-scattering background. In this high-resolution mode the (220) reflection in $Co_2Mn_{0.4}Ti_{0.6}Sn$ shows a clear splitting of the (220) reflection which reveals the phase separation into two Heusler compounds with a slightly different lattice constant as shown in Fig. 6.

B. Magnetic properties

Co_2-based Heusler compounds that are predicted to be half-metallic ferromagnets show a Slater-Pauling behavior of the magnetization which means that the saturation magnetization scales linearly with the number of valence electrons.[24–26] This results in a theoretical magnetic moment of 2 μ_B/f.u. for Co_2TiSn at $T=0$ K which increases linearly

TABLE I. Composition of both phases of $Co_2Mn_{1-x}Ti_xSn$ according to EDX measurements.

x	Mn-rich phase	Ti-rich phase
0.2	Co_2MnSn	$Co_2Mn_{0.56}Ti_{0.43}Sn$
0.4	$Co_2Mn_{0.98}Ti_{0.02}Sn$	$Co_2Mn_{0.26}Ti_{0.74}Sn$
0.5	Co_2MnSn	$Co_2Mn_{0.17}Ti_{0.83}Sn$
0.6	Co_2MnSn	$Co_2Mn_{0.2}Ti_{0.8}Sn$
0.8	$Co_2Mn_{0.4}Ti_{0.6}Sn$	$Co_2Mn_{0.05}Ti_{0.95}Sn$

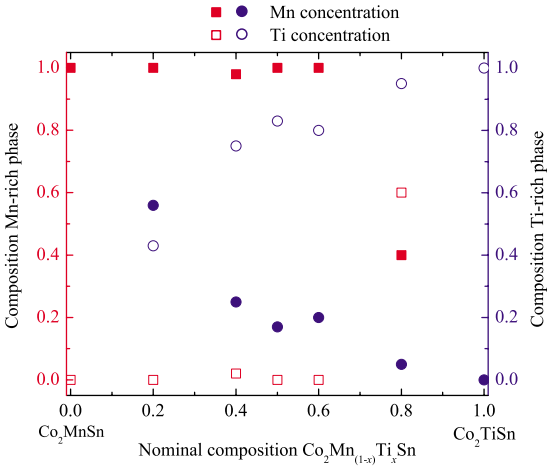

FIG. 4. (Color online) Composition diagram of the two phases. Given are the Mn and Ti concentrations $(1-x)$ and x, respectively, relative to the pure phases. The Co and Sn distributions are constant over the whole composition range and therefore omitted here.

up to 5 μ_B for Co_2MnSn with increasing Mn content. The saturation magnetization of the phase-separated compounds was investigated by SQUID magnetometry. Field-dependent measurements were carried out with an induction field from −5 to 5 T at 5 K.

The compounds show a soft magnetic behavior which is typical for Heusler compounds. Figure 7(a) reveals that the saturation magnetization follows the Slater-Pauling rule. The phase separation does not show any effects on the total magnetic moment of the compounds. However, the reduced magnetic moment for $x=0.8$ may be due to crystallographic disorder within each phase which is below the detection limit of the XRD method. Furthermore, the temperature dependence of the magnetization was studied with an external field of $\mu_0 H = 0.1$ T. According to the hysteresis loops the samples are not yet completely saturated at this field, however, experimental results indicated that the effects which originate from the phase separation could be best observed at $\mu_0 H = 0.1$ T. The temperature-dependent normalized magnetization measurements are shown in Fig. 8.

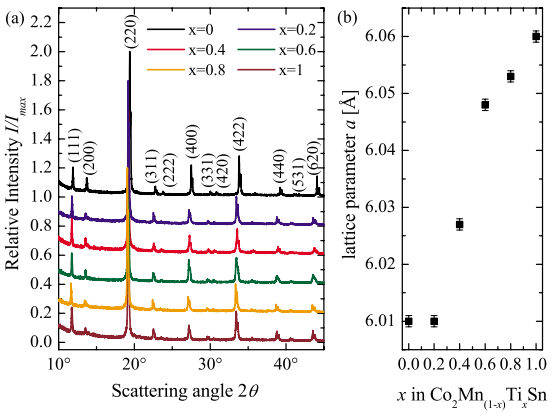

FIG. 5. (Color online) (a) X-ray diffraction patterns of $Co_2Mn_{1-x}Ti_xSn$ measured with Mo $K\alpha$ radiation. (b) Lattice constants determined by Rietveld refinement.

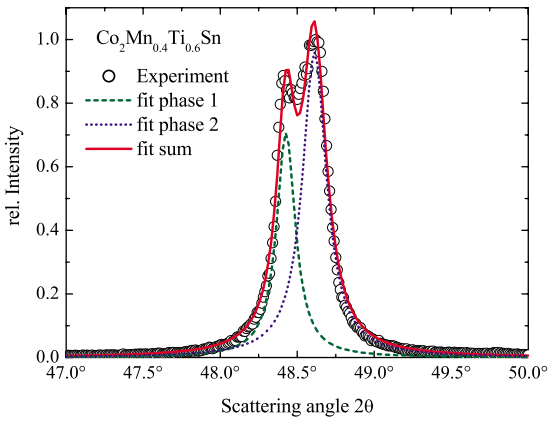

FIG. 6. (Color online) X-ray diffraction of the (220) reflection of $Co_2Mn_{0.4}Ti_{0.6}Sn$.

The magnetic moment remains nearly constant until the Curie temperature of the Ti-rich phase is reached. Since the investigated material contains two magnetic phases a reduction in the magnetization to a finite value at T_C of the Ti-rich phase is observed as displayed in Fig. 8(a). The residual magnetization can be attributed to the Mn-rich phase and decreases to zero at its T_C of this phase (T_C of Co_2TiSn and Co_2MnSn are 355 K and 830 K, respectively[27,28]). The experimental values were determined by an extrapolation of the data according to a mean-field approach (MFT) as described in Ref. 29. Figure 8(b) shows the MFT fits for the sample with $x=0.4$, the Curie temperature of the Ti-rich and the Mn-rich phase are ≈640 K and ≈730 K, respectively. The values for the remaining samples are summarized in Fig. 7(b). In contrast to the known linear trend of T_C for Co_2-based Heusler compounds as a function of valence electrons (dashed line)[13] it can be seen that T_C of the Ti-enriched phase is shifted to lower values whereas it is shifted to higher values for the Mn-enriched phase. Higher amounts of Mn in the sample lead to an elevated T_C of the Ti-enriched phase because the Mn concentration in this phase is increased

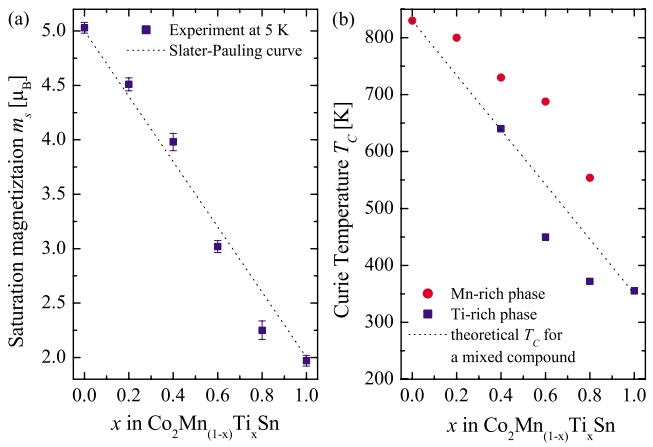

FIG. 7. (Color online) (a) Saturation magnetization m of $Co_2Mn_{1-x}Ti_xSn$ at 5 K. The compounds show a Slater-Pauling behavior. (b) Curie temperature T_C for the Mn-rich and the Ti-rich phases. The dashed lines denote the linear trend which is expected for a mixed compound.

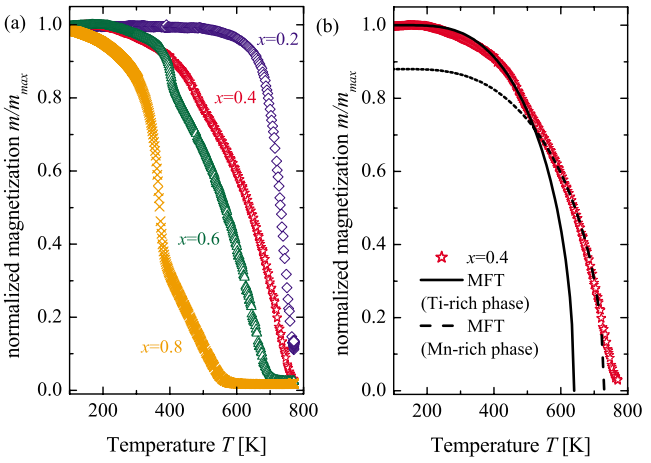

FIG. 8. (Color online) (a) Temperature-dependent magnetization of $Co_2Mn_{1-x}Ti_xSn$. The measurements were performed in an induction field of 0.1 T. (b) Values of T_C for $x=0.4$ according to a mean-field approach are ≈640 K for the Ti-enriched phase and ≈730 K for the Mn-enriched phase.

(compare Sec. III A). The same behavior is observed for the Mn-rich phase since the Ti content in this phase decreases. In addition, T_C of each phase was estimated based on the EDX results assuming a linear variation in T_C with composition. A comparison of these values with the experimental results found by the magnetic measurements is given in Table II. The difference between the T_C determined by SQUID magnetometry and estimated from the EDX data originate from the error with which the EDX data are tainted and from slight deviations from the linear dependence of T_C on the number of valence electrons which is observed for single-phase Heusler compounds.[26] The general trend is well reproduced by this simple approximation.

C. Transport properties

The electrical resistivity for temperatures from 2 to 400 K was obtained by ac four-probe method. Figure 9 shows the temperature dependence of the resistivity and reveals a typical metallic behavior in this temperature range. The resistivity varies nonlinearly with the composition but it is in the same order of magnitude for all compounds with the excep-

TABLE II. Curie temperatures of both phases of $Co_2Mn_{1-x}Ti_xSn$. The values estimated from the EDX results are compared with the values determined by magnetic measurements.

	Mn-rich phase		Ti-rich phase	
	T_C (K)		T_C (K)	
x	(EDX)	(SQUID)	(EDX)	(SQUID)
0.2	830	800	680	
0.4	830	730	500	640
0.6	830	688	400	450
0.8	600	554	360	372

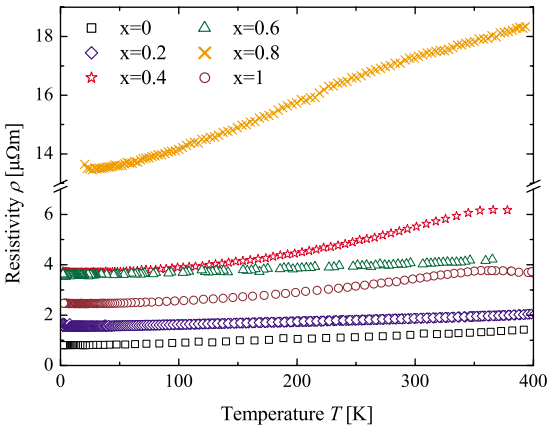

FIG. 9. (Color online) Electrical resistivity of $Co_2Mn_{1-x}Ti_xSn$.

tion of $Co_2Mn_{0.2}Ti_{0.8}Sn$. For this compound the resistivity is larger by a factor of 10. This may result from the fragility of this particular sample which shows distinct cracks. Since the sample exhibits very sharp phase boundaries, strain is introduced to the material leading to the observed brittleness.

The thermal conductivity κ_{tot} was studied in the temperature range between 2 and 300 K to evaluate the possible application of the phase separation as a method to optimize the thermal properties of thermoelectric materials based on Heusler compounds [see Fig. 10(a)]. At low temperatures the thermal conductivities increase steeply with temperature, a maximum is reached between 50–70 K. Above 100 K a weak linear increase with temperature is observed. The thermal conductivity is composed of an electronic contribution κ_e and of a lattice contribution κ_l. To study the impact of the phase separation on the thermal properties, κ_l needs to be separated. The electronic contribution κ_e is calculated based on the electrical-resistivity data according to the Wiedemann-Franz law $\kappa_e = \sigma LT$ with σ the electrical conductivity, L Lorenz number, and the temperature T. By subtraction of κ_e from κ_{tot}, the lattice thermal conductivity κ_l is obtained as displayed in Fig. 10(b). In general, κ_l shows a classical behavior determined by long-wave acoustic phonons with a maximum in the low-temperature range and a plateau at higher temperatures due to the effect of optical phonons. It is remarkable that the value of κ_l is reduced from 5 W/Km for single phase Co_2TiSn to 2–3 W/Km for the phase separated compounds at 300 K. This reduction in ≈50% can only be explained by the combination of different phonon-scattering processes. Grain and phase boundary scattering occurs at the interface between Co_2TiSn and Co_2MnSn. A highly disordered and maybe less dense boundary layer can be assumed which leads to the increased grain boundary resistance both at low and high temperatures.[30] These intergrain layers are not likely to be of uniform thickness since the grains have irregular shapes. The difference in the lattice parameter between Co_2MnSn and Co_2TiSn may also lead to stain effects at the phase boundaries which affects κ_l. Furthermore, κ_l is sensitive to mass fluctuation scattering due to the difference in the atomic masses of Mn and Ti.

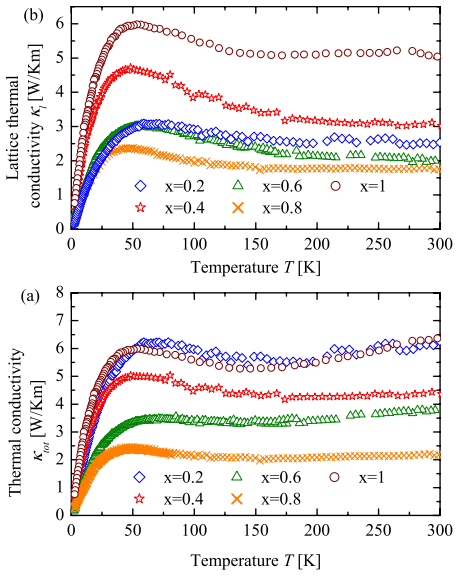

FIG. 10. (Color online) (a) Total thermal conductivity and (b) lattice thermal conductivity of $Co_2Mn_{1-x}Ti_xSn$.

TABLE III. Ratio of the electronic and the lattice contribution to the thermal conductivity.

x	κ_e/κ_l
0.2	1.55
0.4	0.43
0.6	0.91
0.8	0.25

For an application of the phase separation in thermoelectric materials, the ratio of κ_e and κ_l needs to be adjusted. For an optimization of the thermoelectric figure of merit, a ratio of 0.5 is proposed.[31] Table III displays the calculated values of κ_e/κ_l. This ratio changes nonlinearly with composition. In principle, it is possible to adjust the thermal conductivity by choosing the optimal composition with the appropriate microstructure.

Figure 11 shows the Seebeck coefficient that was measured for temperatures ranging from 2 to 400 K. The values decrease with increasing temperature. The Seebeck coefficients for single phase Co_2MnSn and Co_2TiSn at 400 K are −37 μV/K and −50 μV/K, respectively. For the phase-separated compounds the Seebeck effect is lowered with the exception of $Co_2Mn_{0.6}Ti_{0.4}Sn$. In this compound the high Seebeck coefficient of −50 μV/K is retained.

IV. SUMMARY

The phase separation of $Co_2Mn_{1-x}Ti_xSn$ into the Heusler compounds Co_2MnSn and Co_2TiSn was investigated thoroughly. Pictures of the microstructure were obtained by EDX spectroscopy. Its size and shape can be tuned by changes in the Mn/Ti ratio. XRD revealed a splitting of the reflections which is attributed to the different lattice constants of both phases. Two magnetic phase transitions were observed which

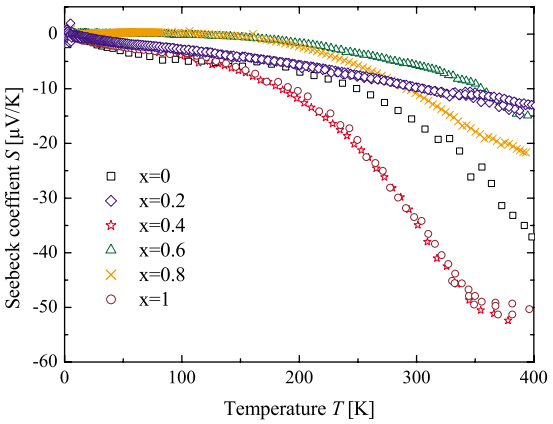

FIG. 11. (Color online) Seebeck coefficients of $Co_2Mn_{1-x}Ti_xSn$.

can be correlated with the different Curie temperatures of the phases. The impact of the phase separation on the transport properties was studied in particular. A reduction in the thermal lattice conductivity of up to ≈50% was found. This opens a new way to tune Heulser compounds for thermoelectric application and to overcome the problem of their comparatively high thermal conductivity. We suggest to transfer the phenomenon to semiconducting Half-Heusler compounds with high Seebeck coefficients. Aside from that, one can take advantage of the phase separation in the field of spintronics. The tunnel magnetoresitance ratio of devices with an IrMn pinning layer decreases dramatically above a critical annealing temperature. This is attributed to an interdiffusion of Mn into the spin-polarized electrodes. The introduction of the half-metallic ferromagnet Co_2TiSn into TMR devices could, therefore, lead to an enhanced temperature stability, which is particularly important for an industrial application of TMR-based devices. Furthermore, the preparation of superlattices composed of Co_2MnSn and Co_2TiSn should be easily possible without any interdiffusion effects during annealing processes. An almost perfect lattice match is a further advantage.

ACKNOWLEDGMENTS

Financial support by the Deutsche Forschungsgemeinschaft (DFG) (Research unit FOR 559, project P 01), the Stiftung Rheinland-Pfalz für Innovation (Project 863), and the Graduate School of Excellence "Material Science in Mainz" MAInZ is gratefully acknowledged.

*felser@uni-mainz.de

[1] R. A. de Groot, F. M. Mueller, P. G. van Engen, and K. H. J. Buschow, Phys. Rev. Lett. **50**, 2024 (1983).
[2] J. M. D. Coey, M. Venkatesan, and M. A. Bari, *Half-metallic ferromagnets*, Lecture Notes in Physics Vol. 595 (Springer-Verlag, Heidelberg, 2002).
[3] C. Felser, G. H. Fecher, and B. Balke, Angew. Chem., Int. Ed. **46**, 668 (2007).
[4] K. Inomata, N. Ikeda, N. Tezuka, R. Goto, S. Sugimoto, M. Wojcik, and E. Jedryka, Sci. Technol. Adv. Mater. **9**, 014101 (2008).
[5] J. Kübler, A. R. Williams, and C. B. Sommers, Phys. Rev. B **28**, 1745 (1983).
[6] M. Kallmayer, H. J. Elmers, B. Balke, S. Wurmehl, F. Emmerling, G. H. Fecher, and C. Felser, J. Phys. D **39**, 786 (2006).
[7] B. Balke, G. H. Fecher, H. C. Kandpal, C. Felser, K. Kobayashi, E. Ikenaga, J.-J. Kim, and S. Ueda, Phys. Rev. B **74**, 104405 (2006).
[8] G. H. Fecher and C. Felser, J. Phys. D **40**, 1582 (2007).
[9] P. Klaer, M. Kallmayer, C. G. F. Blum, T. Graf, J. Barth, B. Balke, G. H. Fecher, C. Felser, and H. J. Elmers, Phys. Rev. B **80**, 144405 (2009).
[10] I. Galanakis, J. Phys.: Condens. Matter **16**, 3089 (2004).
[11] P. J. Webster and K. R. A. Ziebeck, in *Alloys and Compounds of d-Elements with Main Group Elements, Part 2*, Landolt-Börnstein, New Series, Group III Vol. 19, edited by H. P. J. Wijn (Springer-Verlag, Berlin, 1988).
[12] S. Wurmehl, G. H. Fecher, H. C. Kandpal, V. Ksenofontov, C. Felser, H.-J. Lin, and J. Morais, Phys. Rev. B **72**, 184434 (2005).
[13] J. Kübler, G. H. Fecher, and C. Felser, Phys. Rev. B **76**, 024414 (2007).
[14] B. Balke, S. Wurmehl, G. H. Fecher, C. Felser, and J. Kübler, Sci. Technol. Adv. Mater. **9**, 014102 (2008).
[15] R. Shan, H. Sukegawa, W. H. Wang, M. Kodzuka, T. Furubayashi, T. Ohkubo, S. Mitani, K. Inomata, and K. Hono, Phys. Rev. Lett. **102**, 246601 (2009).
[16] N. Tezuka, N. Ikeda, F. Mitsuhashi, and S. Sugimoto, Appl. Phys. Lett. **94**, 162504 (2009).
[17] A. Rajanikanth, D. Kande, Y. K. Takahashi, and K. Hono, J. Appl. Phys. **101**, 09J508 (2007).
[18] V. A. Dinh, K. Sato, and H. Katayama-Yoshida, J. Supercond. Novel Magn. **23**, 75 (2010).
[19] F. F. Li, R. Sharif, L. X. Jiang, X. Q. Zhang, X. F. Han, Y. Wang, and Z. Zhang, J. Appl. Phys. **98**, 113710 (2005).
[20] J. Rodrìgues-Carval, Physica B **192**, 55 (1993).
[21] F. F. Ferreira, E. Granada, C. J. Wilson, S. W. Kycia, D. Bruno, and D. J. Roosevelt, J. Synchrotron Radiat. **13**, 46 (1993).
[22] E. Müller, C. Stiewe, D. Rowe, and S. Williams, *Thermoelectrics Handbook Marco to Nano* (CRC, Boca Raton, 2006).
[23] Q. Design, *Physical Property Measurement System Thermal Transport Option User's Manual* (Quantum Design, San Diego, USA, 2002).
[24] J. Kübler, Physica B **127**, 257 (1984).
[25] I. Galanakis, P. H. Dederichs, and N. Papanikolaou, Phys. Rev. B **66**, 174429 (2002).
[26] G. H. Fecher, H. C. Kandpal, S. Wurmehl, C. Felser, and G. Schönhense, J. Appl. Phys. **99**, 08J106 (2006).
[27] J. Barth *et al.*, Phys. Rev. B **81**, 064404 (2010).
[28] L. Castelliz, Z. Metallkd. **46**, 198 (1955).
[29] C. Kittel, *Introduction into Solid State Physics*, 8th ed. (Wiley, New York, 2005).
[30] P. G. Klemens, Int. J. Thermophys. **15**, 1345 (1994).
[31] C. M. Bhandari, *CRC Handbook of Thermoelectrics* (CRC, Boca Raton, 1995).